American Mineralogist, Volume 80, pages 65–77, 1995

Dozyite, a 1:1 regular interstratification of serpentine and chlorite

STURGES W. BAILEY,† JILLIAN F. BANFIELD,* WILLIAM W. BARKER
Department of Geology and Geophysics, University of Wisconsin, 1215 West Dayton Street, Madison, Wisconsin 53706, U.S.A.

GEORGE KATCHAN
Battle Mountain (Pacific) Ltd., % P. T. Masmindo Eka Sakti, Box 3382/JKT, Jakarta 10002, Indonesia

ABSTRACT

Dozyite is a new mineral species involving regular interstratification of trioctahedral serpentine and trioctahedral chlorite units in a 1:1 ratio. It occurs as colorless crystals in an altered skarn adjacent to the Ertsberg East Cu, Au, and Ag mine in central Irian Jaya, Indonesia. The name is after Jean Jacques Dozy, the Dutch geologist who discovered and named the Ertsberg ore province in 1936. Unit-cell parameters are $a = 5.323(3)$, $b = 9.214(9)$, $c = 21.45(2)$ Å, $\beta = 94.43(6)°$, and $V = 1049(2)$ Å^3. It has space group *Cm*. There is a 21-Å periodicity in the 00*l* and in most other reflections where $k = 3n$. The reflections where $k \neq 3n$ are continuously streaked. Excellent regularity of alternation of the component serpentine and chlorite units is indicated by the coefficient of variation $CV = 0.26$ for the 00*l* reflections. A simplified ideal bulk composition is $(Mg_7Al_2)(Si_4Al_2)O_{15}(OH)_{12}$ with $Z = 2$, halfway between the compositions of the closely associated discrete chlorite (clinochlore) and the discrete serpentine (amesite). We believe the components in this occurrence of dozyite are clinochlore and amesite and that the interstratification was formed during the conversion of early clinochlore to amesite by Al metasomatism. The structure of dozyite contains a I*a* chlorite unit followed by a serpentine 1:1 layer that is in the same position that the lower tetrahedral sheet of a repeating chlorite unit would occupy in the one-layer monoclinic I*aa*-2 chlorite polytype, but rotated 180° so that the octahedral cations alternate I,I,II per 21 Å. The next chlorite unit follows with zero shift of its lower sixfold rings relative to those of the serpentine 1:1 layer.

A second occurrence of dozyite has been recognized in a Cr-rich serpentinite from the Wood Chrome mine in Lancaster County, Pennsylvania. It represents a different polytype, with $\beta = 90°$, and a different composition relative to the Ertsberg material.

INTRODUCTION

Serpentine and chlorite often occur in proximity, either as discrete mixtures of two phases or as components in interstratified sequences. Synthesis data for compositions that overlap show that serpentine is the lower temperature form and chlorite is the higher temperature form (e.g., Yoder, 1952; Nelson and Roy, 1958; James et al., 1976). This is in accord with natural occurrences, where chlorite increases in amount at the expense of serpentine as temperature increases in diagenetic and metamorphic systems.

There is some uncertainty regarding the relation between serpentine and chlorite in Al-rich compositions. Early hydrothermal syntheses by Nelson and Roy (1958) and Gillery (1959) indicated a complete solid solution in serpentine from lizardite, $Mg_3Si_2O_5(OH)_4$, to amesite, $(Mg_2Al)(SiAl)O_5(OH)_4$. The serpentines converted slowly to chlorite above 450 °C at various pressures in the composition range from pennine to an Al-rich phase. Shirozu and Momoi (1972), however, found that compositions from $x = 1.75$ to 2.00 in the system $(Mg_{6-x}Al_x)(Si_{4-x}Al_x)O_{10}(OH)_8$ did not produce a pure, single-phase chlorite at high temperatures and pressures. Chernosky et al. (1988) concluded that present experimental data do not provide reliable information on the stability of chlorite relative to aluminian lizardite with $0.8 < x < 1.5$.

Natural chlorites with $1.5 < x < 1.8$ are rare and for $x > 1.8$ have not been well documented at all. Bailey (1988a) gave approximate limits of Al for Si substitution of 0.4–1.8 atoms per 4.0 tetrahedral positions in chlorites. These limits were based on the data of Foster (1962) and of Bailey and Brown (1962), although compositions in the latter study were based on indirect X-ray spacing-composition graphs. The actual range may be smaller than given. Chernosky et al. (1988) stated that trioctahedral Mg-rich chlorites with $x > 1.5$ do not exist. Bailey (1988b) also suggested that, on the basis of our present knowledge, there may be a compositional gap in serpentines between

† Deceased November 30, 1994.
* To whom reprint requests should be directed.

0003–004X/95/0102–0065$02.00

aluminian lizardite and amesite. The five documented occurrences of amesite cluster closely around the ideal Si_1Al_1 tetrahedral composition. Although Wicks and O'Hanley (1988) showed two samples (nos. 8 and 9 in their Fig. 4) in the compositional range between aluminian lizardite of tetrahedral composition $Si_{2.8}Al_{1.2}$ and amesite with $Si_{2.0}Al_{2.0}$, the compositions of these samples are based on indirect evidence. Samples 8 and 9 are the F and B serpentines described by Bailey and Tyler (1960) from the Tracy mine in northern Michigan. Tetrahedral compositions of $Si_{2.5}Al_{1.5}$ and $Si_{2.25}Al_{1.75}$, respectively, had been obtained using spacing-composition graphs derived from synthesis studies, but Bailey and Tyler (1960) suggested the B serpentine might be less aluminous than what was indicated by the graph because of the relative amounts of forsterite, enstatite, and spinel formed by static heating up to 300 °C. Hall et al. (1976) later showed that the B serpentine contains two phases of differing cell dimensions and, presumably, different compositions. Further study is required before this specimen can be evaluated.

Serpentine-chlorite interstratifications have been studied primarily by X-ray diffraction and TEM methods. Reynolds (1988) pointed out that X-ray characterization by oriented powder slides is difficult because neither component changes its d_{001} value appreciably as a result of heating or solvation tests. The 00*l* peaks of serpentine overlap nearly exactly the even orders of the chlorite 00*l* peaks, provided the compositions are similar. Detection of interstratification thus depends on a detailed comparison of observed and calculated peak intensities and widths. Convincing X-ray evidence for the existence of random interstratifications of 7- and 14-Å components, nevertheless, was provided by Brindley and Gillery (1954), Dean (1983), Bailey (1988c), Walker and Thompson (1990), Moore and Hughes (1991), Hillier and Velde (1992), and Reynolds et al. (1992). The 7-Å component in these samples has been reported variously as serpentine, berthierine, and possibly kaolinite.

Imaging of the component layer thicknesses by HRTEM provides more direct visual evidence for interstratification. Irregular sequences of 7-Å (ferroan lizardite) and 14-Å (trioctahedral chlorite) spacings were shown by Lee and Peacor (1983) to be present in some of the rocks of the Martinsburg shale that are transitional in the conversion of shale to slate at Lehigh Gap, Pennsylvania. Ahn and Peacor (1985) showed a similar random interstratification of berthierine within "brunsvigite chlorite" in a diagenetic suite of Oligocene-Miocene Gulf Coast shale samples at well depths of 2450 and 5500 m. Yau et al. (1988) showed berthierine 1:1 layers to be present within 14-Å chlorite packets in shales from the Salton Sea geothermal field of California at temperatures below 220 °C, but only pure chlorite packets were present above 220 °C. Odin et al. (1988) showed interstratified 7- and 14-Å spacings, as well as thicker packets of each, present in the transformation of odinite to chlorite in several near-shore Recent Quaternary sediments in tropical latitudes. Amouric et al. (1988) observed isolated 1:1 layers randomly interstratified within 14-Å units as well as packets of 1:1 layers within blocks of 14-Å units in pelitic flysch deposits from the Piemontese formations in the western Caribbean mountain system of Venezuela. Jahren and Aagaard (1989) found early-formed 7-Å berthierine transforming diagenetically above 70 °C to chlorite-I*b* (β = 90°) in pore fillings in clastic reservoir rocks offshore from Norway. Jiang et al. (1992) and Slack et al. (1992) found randomly interstratified berthierine-chlorite, both as small numbers of layers of each form and as thicker packets, in the alteration zone of the Kidd Creek massive sulfide deposit in Ontario. The berthierine and chlorite were of similar compositions and were believed to form by replacement of chlorite by berthierine under nonequilibrium retrograde conditions.

The only report of regularly interstratified serpentine-chlorite known to the authors is that of Jiang et al. (1982). They claimed regular interstratification of both "septechlorite" and "swelling chlorite" and antigorite-chlorite in a hydrothermal lens within a serpentinite body in Sichuan Province, China. The d_{001} value reported for both systems was 32 Å, but this is not the correct value for a superlattice of serpentine plus chlorite. Also, the alternation of layers in these specimens can have only local ordering because no higher order 00*l* reflections are present beyond 001 and 002.

The present paper reports a 1:1 regularly interstratified serpentine-chlorite that occurs in crystals coarse enough to permit unequivocal characterization of its nature and of some of its crystallographic features. The crystals occur in a drill core from the Ertsberg East skarn body (Gunung Bijih Timur, or G.B.T., in Indonesian) in the Ertsberg Cu, Au, and Ag ore province of central Irian Jaya, Indonesia. The species name, dozyite, is in honor of Jean Jacques Dozy, the Dutch geologist who discovered and named the Ertsberg ore province in 1936. The name has been approved by the Commission on New Minerals and Mineral Names of the International Mineralogical Association. The name is intended for all 1:1 regular interstratifications of trioctahedral serpentine and trioctahedral chlorite, regardless of the precise compositions of the two trioctahedral components or the structural modification of the chlorite. Important compositional variants outside the Mg-Al system can be indicated by adjectival modifiers. All material available to the authors has been deposited in the Smithsonian National Museum of Natural History, Washington, DC (NMNH no. 170825).

Occurrence

The first occurrence of dozyite to be reported here is in one small segment of a core drilled by the Freeport Indonesia Company. The core is labeled S5-10 at a 674.6-m depth. The core is from an altered skarn in the intermediate ore zone within the G.B.T. or Ertsberg East Complex, located at an elevation of 4200 m in the Carstensz Mountains of central Irian Jaya, Indonesia, about 100 km from the southern coast. The skarn developed by the intrusion of a Plio-Pleistocene quartz monzonite into Tertiary dolomitic limestones and was subject to a series of Si, Fe, and Al metasomatisms and ore mineralizations

TABLE 1. Electron probe analysis of dozyite*

	Oxide		
SiO_2	29.69(0.43)		
Al_2O_3	20.29(0.61)		
MgO	34.74(0.38)		
FeO	1.63(0.12)	or Fe_2O_3	1.81(0.14)
CaO	0.04(0.033)		
Na_2O	0.07(0.094)		
Cl	0.18(0.179)		
K_2O	nil		
Li_2O**	nil		
B_2O_3**	nil		
BeO**	nil		
H_2O**	12.20(1.22)		
Total	98.84		99.02
	Atoms		
Si	4.202	Si	4.182
Al	3.385	Al	3.370
Mg	7.327	Mg	7.293
Fe^{2+}	0.191	Fe^{3+}	0.192
Total	15.105	Total	15.037

Note: oxides given as weight percent (σ).

* Average of 19 analyses. Cameca SX50 microprobe operated at 15 keV and 10 nA. Absorption corrections by the PAP $\phi(\rho,Z)$ method using standards of Evans's muscovite, Rockport fayalite, and synthetic MgO. Atoms on the basis of 42 positive charges for ferrous and ferric cases. Analyst: J. Fournelle.

** Ion probe analysis by L. Riciputi, Oak Ridge National Laboratory. Standard of Day Book Body chlorite.

TABLE 2. Semi-quantitative analytical electron microscope analyses for Mg, Al, and Si

	Clinochlore	Amesite	$Dozyite_{calc}$*	$Dozyite_{EMP}$
Si	3.0	1.1	4.1	4.1
$^{[4]}Al$	1.0	0.9	1.9	1.9
$^{[6]}Al$	1.3	1.0	2.3	1.8
Mg	4.5	1.9	6.4	7.1
Fe^{3+}	n.d.	n.d.	n.d.	0.2
O	10	5	15	15
OH	8	4	12	12

Note: analyses made by energy-dispersive spectrometry; n.d. = not determined.

* The sum of clinochlore + amesite.

(Katchan, 1982). To date six ore bodies have been discovered in an area 6.3 × 6.3 km in the Ertsberg district, involving several different skarns and intrusive bodies.

Minerals associated with dozyite in the drill core are lizardite and chrysotile, pseudomorphic after forsterite, antigorite, amesite, clinochlore, other interstratified serpentine-chlorite phases, magnesite, dolomite, calcite, anhydrite, and chalcopyrite. The core shows a forsterite nodule about 3.0 cm in diameter that has been altered to fine-grained olive green serpentine, primarily lizardite and clinochrysotile (±dolomite and magnesite). This is succeeded outward by a 0.5-cm halo of fine-grained yellow serpentine, primarily clinochrysotile (±dolomite and magnesite), then by a 0.5-cm halo of crystals of intergrown colorless dozyite, colorless to pale green clinochlore, amesite, and other serpentine-chlorite phases (±dolomite), followed by about 1.0 cm of anhydrite to the core boundary. Thin veinlets of calcite and light blue serpentine transect the core, along with scattered specks of chalcopyrite. Adjacent cores contain serpentine, brucite, chlorite, dolomite, magnetite, and sulfides. A calc-silicate suite of monticellite, vesuvianite, calcite, and clintonite occurs 1.6 km away in the open pit of the Ertsberg mine. The crystal structure of a clintonite-1*M* crystal from this pit was refined by MacKinney et al. (1988). These samples were collected in 1978 by one of the authors during field work for a Ph.D. thesis (Katchan, 1982).

The second occurrence of dozyite is in a Cr-rich serpentinite from the Wood Chrome mine in Lancaster County, Pennsylvania (Banfield et al., in preparation). Samples were provided by Robert C. Smith II. Minerals coexisting with chromian dozyite include chromian chlorite-II*bb*, chromian lizardite (types C and D), and chromite. The chromian dozyite appears as mauve sprays and fine interstitial intergrowths peppered with small, aligned chromite inclusions. The chromian dozyite differs significantly from the Ertsberg material. For example, the β angle for Cr-rich material is 90° (indicating a different polytype), and the Al content is much lower. In this paper we report details only for the Ertsberg dozyite. However, reference is made to this second example to illustrate that the formation conditions for regular serpentine-chlorite intergrowths may vary and that dozyite may form with compositions different from that reported for the Ertsberg material.

COMPOSITION AND PHYSICAL PROPERTIES

Table 1 lists an electron microprobe (EMP) analysis of the Ertsberg dozyite, plus ion probe analyses for H, Li, B, and Be. Deletion of small amounts of Ca, Na, and Cl as impurities and allocation of the remainder to a structural formula on the basis of 42 positive charges (14 for serpentine and 28 for chlorite) leads to a bulk composition of $(Mg_{7.33}Al_{1.59}Fe^{2+}_{0.19})^{+1.81}_{9.11}(Si_{4.20}\ Al_{1.80})^{-1.80}_{6.00}O_{15}(OH)_{12}$ on the assumption of Fe^{2+} or to $(Mg_{7.29}Al_{1.55}Fe^{3+}_{0.19})^{+1.80}_{9.03}(Si_{4.18}Al_{1.82})^{-1.82}_{6.00}O_{15}(OH)_{12}$ on the assumption of Fe^{3+}. The latter is preferred because it gives a more integral octahedral occupancy. If the latter bulk composition is distributed in a 1:2 ratio between the serpentine and chlorite components, then the interstratification would be between lizardite $[(Mg_{2.43}Al_{0.52}Fe^{3+}_{0.06})^{+0.60}_{3.01}(Si_{1.39}Al_{0.61})^{-0.61}_{2.00}O_5(OH)_4]$ and clinochloreore $[(Mg_{4.86}Al_{1.04}Fe^{3+}_{0.12})^{+1.20}_{6.02}(Si_{2.78}Al_{1.22})^{-1.22}_{4.00}O_{10}(OH)_8]$. A simplified ideal bulk composition is $(Mg_7Al_2)(Si_4Al_2)O_{15}(OH)_{12}$.

The AEM-determined compositions of coexisting serpentine and chlorite are listed in Table 2. Serpentine and chlorite analyses exhibited considerable variation, primarily because of minor interstratified serpentine in chlorite and vice versa. The clinochlore has a less aluminian composition than what was assumed above, whereas the serpentine has a composition close to that of amesite ($^{[4]}Al/Si \sim 0.8$). The tetrahedral Al-Si ratio for serpentine in Table 2 would match ideal amesite more closely if Fe were considered.

The bulk composition of dozyite determined by EMP analysis is almost exactly halfway between the compositions of the coexisting clinochlore and amesite phases, as determined by AEM, as would be expected if dozyite con-

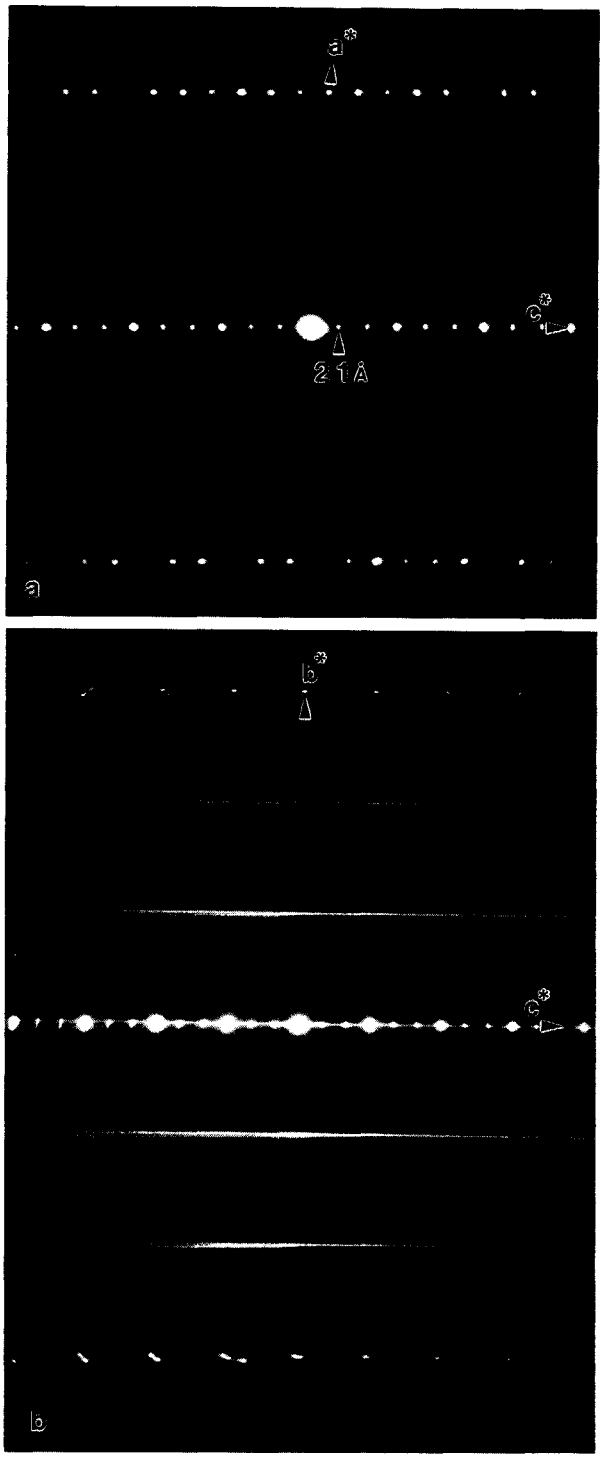

Fig. 1. (**a**) The [010] SAED and (**b**) [100] SAED patterns from dozyite. Note that 00*l* reflections with $l = 3n$ are consistently more intense than those with $l = 3n \pm 1$ and that reflections with $k \neq 3n$ are continuously streaked.

sists of a 50:50 ratio of clinochlore and amesite components. The composition of dozyite was predicted on the basis of interstratification of serpentine and chlorite whose compositions were derived by AEM of the coexisting phases (qualitative Fe assignment based on AEM data). The predicted composition is close to that determined by EMP analysis (Table 2). Additional evidence for the compositions of the two components in dozyite comes from a coexisting 28-Å regular interstratification. HRTEM images of this phase show regular alternation of one chlorite unit with two serpentine units. The bulk composition of this phase, as determined by AEM, falls halfway between those of dozyite and amesite (Banfield et al., 1994). This is only possible if the added serpentine unit has the composition of amesite. Thus, our preferred allocation for dozyite is an interstratification of the two associated phases as $(Mg_{2.00}Al_{0.85}Fe^{3+}_{0.15})^{+1.00}_{3.00}(Si_{1.00}Al_{1.00})^{-1.00}_{2.00}O_5(OH)_4$ and $(Mg_{5.29}Al_{0.70}Fe^{3+}_{0.04})^{+0.80}_{6.03}(Si_{3.18}Al_{0.82})^{-0.82}_{4.00}O_{10}(OH)_8$.

Dozyite crystals in the drill core range up to 2.0 mm in diameter and are intergrown with amesite, clinochlore, and other serpentine-chlorite interstratified phases as tabular (001) wedges, whorls, and platelets in a tight network. The dozyite crystals are colorless, whereas the other interstratified phases and the discrete amesite and clinochlore are colorless to pale green. The streak of dozyite is white and the luster nacreous. The hardness is about 2.5. The density measured with a Berman balance is 2.66 g/cm³ vs. 2.66 calculated with $Z = 2$.

Optically, dozyite crystals are essentially uniaxial positive, although there is a slight separation of the isogyres to a biaxial nature ($2V$ under 5°). The refractive indices measured in Na(D) light are $\alpha = \beta = 1.575(1)$ and $\gamma = 1.581(1)$. The optic plane is parallel to (010). The orientation is $Y = \mathbf{b}$ and Z:**c** = 4° (in obtuse angle β). Dispersion is very weak. Pleochroism is characterized as $X = Y$ = colorless; Z = very pale tan in thick crystals. The compatibility index $1 - (K_p/K_c) = 0.023$ = excellent.

X-RAY AND ELECTRON DIFFRACTION RESULTS

Because of the small quantity of material available and the intergrown nature of dozyite with amesite, clinochlore, and other serpentine-chlorite interstratifications, no powder diffractometer mounts were attempted. X-ray study was concentrated on single crystals. Selected-area electron diffraction (SAED) patterns were obtained from transmission electron microscope specimens thinned to electron transparency either by Ar ion milling or ultramicrotome techniques. SAED patterns provided single-crystal diffraction information from submicrometer-wide areas.

More than 100 crystals of dozyite and associated phyllosilicates were examined by single-crystal X-ray precession, Weissenberg, or diffractometer methods, and numerous crystals (eight ion-milled and several microtomed samples) were examined using SAED. X-ray diffraction patterns revealed that 00*l* reflections are of equal breadth and form a rational series from 001 at 21.386 Å to 0,0,30 at 0.713 Å. SAED patterns show 00*l* reflections with $l = 3n$ generally more intense than those with $l = 3n \pm 1$ (Fig. 1). The latter are not of observable intensity beyond $n = 4$ on Debye-Scherrer X-ray patterns, but some beyond $n = 4$ are visible in SAED patterns and are recorded

also by slow scans on a single-crystal X-ray diffractometer. In all, 24 reflections were observed from 001 to 0,0,30.

In order to test the rationality of the 00*l* sequence, a crystal was mounted on a Syntex $P2_1$ single-crystal diffractometer, and each 00*l* reflection in turn was centered on the four circles of the instrument. The 2θ values of 00*l* and $00\bar{l}$ were averaged and converted to *d* values, which are listed in Table 3, along with their observed integrated intensities (I_{obs}) and corrected structure amplitudes (F_{obs}). The 001 reflection was cut out by the beam stop (2θ = 1.90° for Mo$K\alpha$ radiation) and was observed only on Gandolfi films with Fe$K\alpha$ radiation and in SAED patterns. The intensities of eight other observed reflections proved too small to allow centering. The average d_{001} value is $\bar{X}$ = 21.381 Å (compared with 21.386 Å calculated from the cell parameters). The coefficient of variation $CV = 100s/\bar{X}$, where

$$s = \left[\frac{\Sigma (X_i - \bar{X})^2}{n - 1}\right]^{1/2}$$

of the $X_i = ld_{00l}$ values for the 15 centered reflections is 0.26. This qualifies the interstratification as having sufficient regularity of alternation ($CV < 0.75$) to warrant species status, according to the standards of the AIPEA Nomenclature Committee (Bailey, 1982). The reflections do not change position on solvation with glycerol or heating to 400 °C.

The bulk chemical composition does not give the distribution of elements between the component layers, although we favor an alternation of amesite and clinochlore. Because the X-ray scattering powers of Mg, Al, and Si are similar, the 00*l* intensities can be calculated for a 1:1 regular alternation on the assumption of tetrahedral and octahedral compositions that are identical in the component layers. The *z* heights used for atomic planes of the chlorite component were those of II*bb*-2 clinochlore (Zheng and Bailey, 1989), and the distances between these planes also were used to build up a serpentine 1:1 layer, with all *z* heights adjusted for $c \sin \beta$ = 21.386 Å. The resulting calculated F_{00l} values are shown in Table 3.

No correction of the intensities for Lorentz-polarization and absorption factors had been made at this stage, and a plot of I_{obs}/F^2_{calc} vs. sin θ resulted in a distribution of data points typical of errors of that type, but with $l \neq 3n$ and $l = 3n$ points separated from one another. The $l \neq 3n$ points formed a descending curve from lowest θ to θ = 10°, then they leveled off. The $l = 3n$ points, however, plotted away from this curve by an amount that could be correlated with the ratio F^2_{calc}(amesite) to F^2_{calc}(dozyite). This indicated that this crystal of dozyite was intergrown with approximately 20% of amesite, with the 7-Å series of amesite 00*l* reflections superimposed on the 21-Å 00*l* series of dozyite. Some of the most intense 20*l* reflections of amesite also could be identified as present on precession films, although these in general overlapped only a few dozyite 20*l* reflections because of the difference in β angles (94.4° vs. 90°). The contribution of 20% amesite to each 00*l* reflection of dozyite with $l = 3n$ was calculated and used to modify the raw intensity values. The curve for the $l \neq 3n$ plot vs. sin θ then was converted to a straight line to correct for the systematic error present, and all corrected intensities were scaled to F^2_{calc} of dozyite (Table 3). The residual, *R*, of 7.5% between F_{obs} and F_{calc}, without any refinement of *z* heights of the atomic planes, indicates a successful correction procedure and confirms a regular alternation of serpentine and chlorite units in the interstratification.

TABLE 3. Dozyite basal reflections, 00*l**

l	d_{obs} (Å)	d_{calc} (Å)	I_{obs}	F_{obs}	F_{calc}
1	(21.4)	21.386	—	—	32.1
2	10.700	10.693	4435	66.6	63.5
3	7.116	7.129	14805	121.7	125.3
4	5.311	5.346	11099	105.4	112.1
5	4.301	4.277	11988	109.5	120.0
6	3.564	3.564	47211	217.3	224.5
7	3.054	3.055	8551	92.5	101.3
8	2.671	2.673	6993	83.6	85.8
9	2.378	2.376	3750	61.2	47.4
10	2.131	2.139	5210	72.2	65.0
11	1.948	1.944	2552	50.5	57.7
12	1.784	1.783	2108	45.9	39.6
13	(1.645)	1.645	1614	40.2	35.7
14	(1.531)	1.528	509	22.4	18.9
15	1.426	1.426	9254	96.2	97.6
16	(1.339)	1.337	156	12.5	10.3
17	(1.260)	1.258	213	14.6	16.1
18	1.188	1.188	6448	80.3	83.8
19	(1.128)	1.126	137	11.7	11.0
20	—	1.069	0	0	5.7
21	1.018	1.018	4020	63.4	54.2
22	—	0.972	0	0	0
23	—	0.930	0	0	0
24	0.891	0.891	3468	58.9	50.0
25	—	0.855	0		
26	—	0.823	0		
27	—	0.792	0		
28	(0.765)	0.764	37		
29	(0.737)	0.737	43		
30	(0.713)	0.713	47		

* Observed *d* values obtained by centering reflections on single-crystal diffractometer. Reflections with *d* values in parentheses either were blocked by the beam stop or were too weak to permit repetitive-scan centering. Values given are based on single scans. Observed *F* values obtained by correcting observed intensities for Lorentz-polarization factors, absorption, and amesite impurity, then scaling to ΣF^2_{calc}. The F_{calc} values are based on unrefined *z* coordinates.

The 21-Å periodicity is evident not only in the spacings of the 00*l* reflections but also in those of most of the other $k = 3n$ reflections (Fig. 2). However, the $k \neq 3n$ reflections were continuously streaked for all crystals examined (Fig. 1b). The streaking is due to random displacements of $\pm b/3$ between the basal O atoms of the component layers, whereas the sharpness of the $k = 3n$ spectra (Fig. 1a) is due to the fact that the diffracted contributions to the latter from the octahedral cations and anions (which repeat at intervals of $b/3$ in the structure) are not affected by these random displacements. Weissenberg and precession X-ray photographs can be indexed best with a monoclinic-shaped unit cell, with $\beta \sim 94.4°$. This corresponds to a resultant layer shift of $-a_1/3$ per 21-Å sequence along **c** (β_{ideal} = 94.73°). The apparent symmetry is $C2/m$, taking into account the lack of discrete $k \neq 3n$ reflections, but because of the polar serpentine component, the actual symmetry must be Cm or $C1$.

TABLE 4. Powder pattern of dozyite

I_{obs}	I_{calc}	d_{obs}	d_{calc}	*hkl*	I_{obs}	I_{calc}	d_{obs}	d_{calc}	*hkl*
15	24	21.4	21.386	001	10	3	1.740	1.738	139
15	24	10.7	10.693	002		2		1.732	2,0,$\bar{10}$
100	109	7.1	7.129	003	5	3	1.705	1.706	209
15	24	5.31	5.346	004		5		1.699	1,3,$\bar{10}$
60	—	4.61	4.607	0,2,11	5	4	1.635	1.636	1,3,10
15	19	4.30	4.277	005		2		1.629	2,0,$\bar{11}$
80	78	3.560	3.564	006	20	5	1.603	1.606	2,0,10
5	8	3.052	3.055	007		9		1.599	1,3,$\bar{11}$
	5		2.673	008	70	34	1.536	1.536	33$\bar{1}$
20	4	2.660	2.654	200		22		1.536	060
	11		2.651	13$\bar{1}$		5		1.503	332
	8		2.609	201	25	7	1.501	1.501	063
25	20	2.608	2.603	13$\bar{2}$		5		1.500	33$\bar{4}$
	42		2.556	132		1		1.478	333
40 B	18	2.557	2.552	20$\bar{3}$	1	1	1.478	1.476	064
	5		2.530	202		1		1.475	33$\bar{5}$
15	8	2.528	2.523	13$\bar{3}$		2		1.454	1,3,12
	19		2.460	133		2		1.449	2,0,$\bar{13}$
20	11	2.460	2.454	20$\bar{4}$	2B	1	1.450	1.448	334
	26		2.426	203		1		1.445	065
60	57	2.427	2.418	13$\bar{4}$		1		1.444	33$\bar{6}$
2	3	2.377	2.376	009	10	3	1.426	1.426	0,0,15
	7		2.344	134		2		1.413	335
10	9	2.240	2.337	20$\bar{5}$	15	3	1.411	1.410	066
	9		2.307	204		2		1.408	33$\bar{7}$
20	18	2.301	2.298	13$\bar{5}$		7		1.375	1,3,13
	2		2.220	135	10	3	1.375	1.370	2,0,$\bar{14}$
3B	2	2.185	2.181	205		1		1.323	261
	3		2.172	13$\bar{6}$		2		1.323	40$\bar{3}$
1	2	2.140	2.139	0,0,10	10B	1	1.322	1.318	401
	8		2.092	136		2		1.316	26$\bar{3}$
8	5	2.090	2.085	20$\bar{7}$		1		1.302	26$\bar{4}$
	6		2.054	206		3		1.298	2,0,$\bar{15}$
10	12	2.055	2.045	13$\bar{7}$	5	1	1.300	1.298	263
	17		1.968	137		2		1.296	40$\bar{5}$
20	10	1.968	1.961	20$\bar{8}$					
	7		1.931	207					
15	12	1.929	1.923	13$\bar{8}$					
	4		1.850	138					
4	2	1.849	1.842	20$\bar{9}$					
	1		1.814	208					
1	2	1.810	1.807	13$\bar{9}$					
1	1	1.783	1.782	0,0,12					

Note: units of measure for *d* are ångströms. Pattern of diced crystal mounted in a Gandolfi camera, 114.6-mm diameter, graphite-monochromatized Fe$K\alpha$ radiation. Indexing by comparison with single-crystal data; intensities estimated visually.

TABLE 5. *R* values for nine possible structural models of dozyite*

Polytype	Oct. cation set	*R* (%)
Type I chlorite component (I,I or II,II octahedral cation sets occupied)		
I*aa*-2	I,I,II	25.0
I*bb*-1	I,I,II	59.8
I*ba*-2	II,II,I	52.4
Type II chlorite component (I,II or II,I octahedral cation sets occupied)		
II*aa*-1A	I,II,I	50.5
II*aa*-1B	I,II,II	41.2
II*bb*-2A	II,I,I	64.2
II*bb*-2B	II,I,II	60.6
II*ba*-1A	I,II,I	59.2
II*ba*-1B	I,II,II	42.1

* F_{calc} values calculated on basis of ideal, unrefined atomic coordinates. F_{obs} values not corrected for Lorentz-polarization or absorption factors. *R* based on 47 composite 20*l* and 20*l* reflections.

Unit-cell parameters of $a = 5.323(3)$, $b = 9.214(9)$, $c = 21.45(2)$ Å, $\alpha = 90.05(7)$, $\beta = 94.43(6)$, $\gamma = 89.92(7)°$, and $V = 1049(2)$ Å^3 were determined by least-squares fitting of 15 medium-angle reflections (23–47° 2θ, Mo$K\alpha$ radiation) centered on a Syntex $P2_1$ single-crystal diffractometer. A Gandolfi X-ray powder pattern is listed in Table 4, indexed by cross reference to single-crystal data. Not all the 00*l* reflections observed on single-crystal patterns are visible on the powder pattern.

STRUCTURAL DETERMINATION

The strong 21-Å periodicity observed for the $k = 3n$ reflections requires a regular alternation along c of octahedral cations between the I and II sets of possible positions in a sequence such as I,II,I; I,II,II; or I,I,II for the three octahedral sheets of the assemblage (two for chlorite followed by one for serpentine) (Bailey, 1988d). All other possible three-sheet octahedral sequences are equivalent

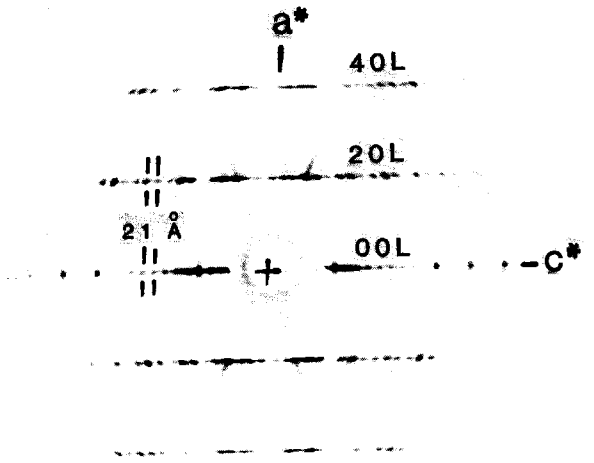

Fig. 2. The a*-c* precession pattern from a dozyite single crystal.

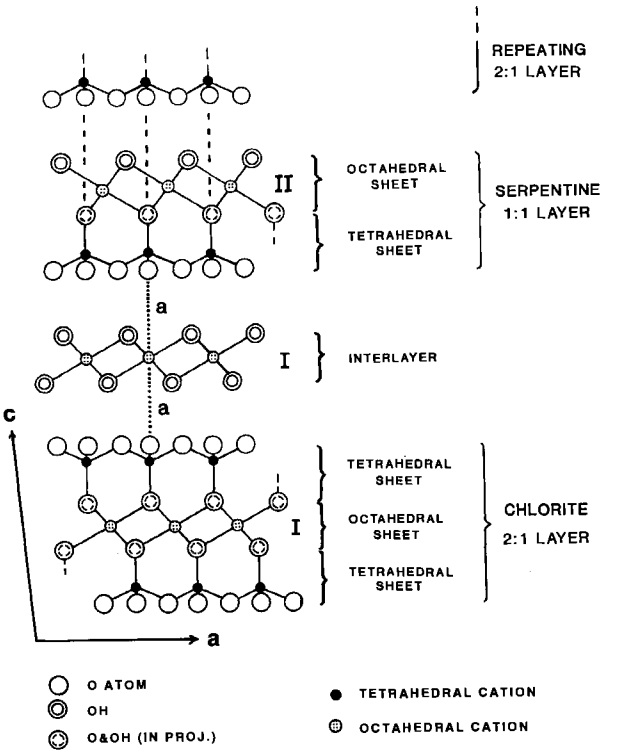

Fig. 3. A I*aa*-2 structural model for dozyite. The vertical alignment of interlayer and tetrahedral cations is indicated by the "a" symbols.

to these three after a 180° rotation about c*. Nine structural models giving a resultant symmetry of *Cm* are possible for dozyite, with the mirror plane of each component layer coincident in (001) projection. Each model provides alternation of octahedral cations according to one of the three sequences above (or equivalents), reasonable bond lengths between all atoms, and $-a_1/3$ net shifts per 21-Å sequence, and each preserves interlayer H bond contacts. The models differ according to the chlorite structural type (I*a*, I*b*, II*a*, or II*b*), the octahedral cation sequence, and the relative positions of the serpentine and chlorite units. In all nine models the constraint of H bonding requires the sixfold rings of the overlying serpentine 1:1 layer to be in the same position that the lower tetrahedral sheet of a repeating chlorite 2:1 layer would occupy in the standard one-layer monoclinic chlorite polytypes of Bailey and Brown (1962). The tetrahedral cations of the serpentine 1:1 layer then are in either the *a* or *b* position relative to the chlorite interlayer cations below. The six unique tetrahedral-interlayer-tetrahedral configurations can be described as I*aa*-2, I*ba*-2 (=I*ab*-1), II*aa*-1, II*bb*-2, I*bb*-1, and II*ba*-2 (=II*ab*-1) in the revised terminology of Bailey (1988d). For the first four models listed above, the resultant $-a_1/3$ shift for the structure as a whole is achieved within the chlorite structural unit, and the sixfold rings of the repeating chlorite 2:1 layer must be positioned with zero shift relative to the serpentine sixfold rings below. In the I*bb*-1 and II*ba*-2 models the chlorite unit has $\beta = 90°$, however, and the net $-a_1/3$ shift must be achieved at the serpentine-chlorite interface. For the three type I configurations above, the only octahedral cation sequence possible is I,I,II (chlorite cations in I,I and those of serpentine in II orientations). Sequence II,II,I is equivalent by rotation. For the three type II configurations, both I,II,I (or II,I,II) and I,II,II (or II,I,I) octahedral cation sequences are possible. That is, the serpentine 1:1 layer can be rotated by 180° relative to the chlorite unit.

Intensities were calculated for each model using ideal atomic coordinates derived from appropriately oriented transparencies of the serpentine and chlorite structures. The origin was placed at octahedral cation M1 in the 2:1 layer. The continuously streaked $k \neq 3n$ reflections indicate shifts of $-a/3$ are taking place along all three pseudohexagonal **a** axes in random fashion in the actual structure, equivalent to random ±120° rotations of the units. In order to facilitate comparison of F_{calc} and F_{obs}, this random rotation can be simulated by averaging the F_{calc} values of the three reflections that would be superimposed by ±120° rotations. This is a relatively minor correction because these reflections are pseudohexagonal equivalents and have comparable intensities. The residual *R* values between F_{obs} and F_{calc} for 47 composite 20*l* reflections of this type are shown in Table 5 for the nine models. Model I*aa*-2 is clearly the best fit, and the *R* of 25% is reasonable in view of the lack of correction to F_{obs} for absorption and Lorentz-polarization effects, the usage of unrefined atomic coordinates, and lack of correction of F_{obs} for the overlap of amesite for some reflections. This model (Fig. 3) contains a I*a* chlorite unit. This is

TABLE 6. Unrefined atomic coordinates of dozyite

Atom	x	y	z	Atom	x	y	z
M1	0.0000	0.0000	0.0000	O4	−0.0076	0.0000	0.5112
M2	0.0000	0.3333	0.0000	O5	0.2424	0.2500	0.5112
OH1	0.3486	0.0000	0.0493	T2	0.0011	0.1667	0.5388
O1	0.3493	0.3333	0.0513	O6	0.0249	0.1667	0.6153
T1	0.3731	0.3333	0.1278	OH6	0.5254	0.0000	0.6173
O2	0.3817	0.5000	0.1554	M5	0.2075	0.0000	0.6667
O3	0.1317	0.2500	0.1554	M6	0.2075	0.3333	0.6667
OH2	0.0892	0.0000	0.2865	OH7	−0.1113	0.0000	0.7135
OH3	0.0892	0.3333	0.2865	OH8	−0.1113	0.3333	0.7135
M3	−0.0630	0.5000	0.3333	O7	0.0962	0.0000	0.8446
M4	−0.0630	0.1667	0.3333	O8	0.3461	0.2500	0.8446
OH4	0.7850	0.0000	0.3801	T3	0.1048	0.1667	0.8722
OH5	0.2850	0.1667	0.3801	O9	0.1286	0.1667	0.9487
				OH9	0.6291	0.0000	0.9507

followed by a serpentine 1:1 layer that is in the same position that the lower tetrahedral sheet of a repeating chlorite unit would occupy in the one-layer monoclinic I*aa*-2 chlorite polytype, but rotated 180°. Thus, the serpentine tetrahedral cations are in the *a* positions relative to the interlayer cations below, and the serpentine sixfold rings are over the 2 positions of the interlayer. The octahedral cation sets alternate as I,I,II per 21 Å. The re-

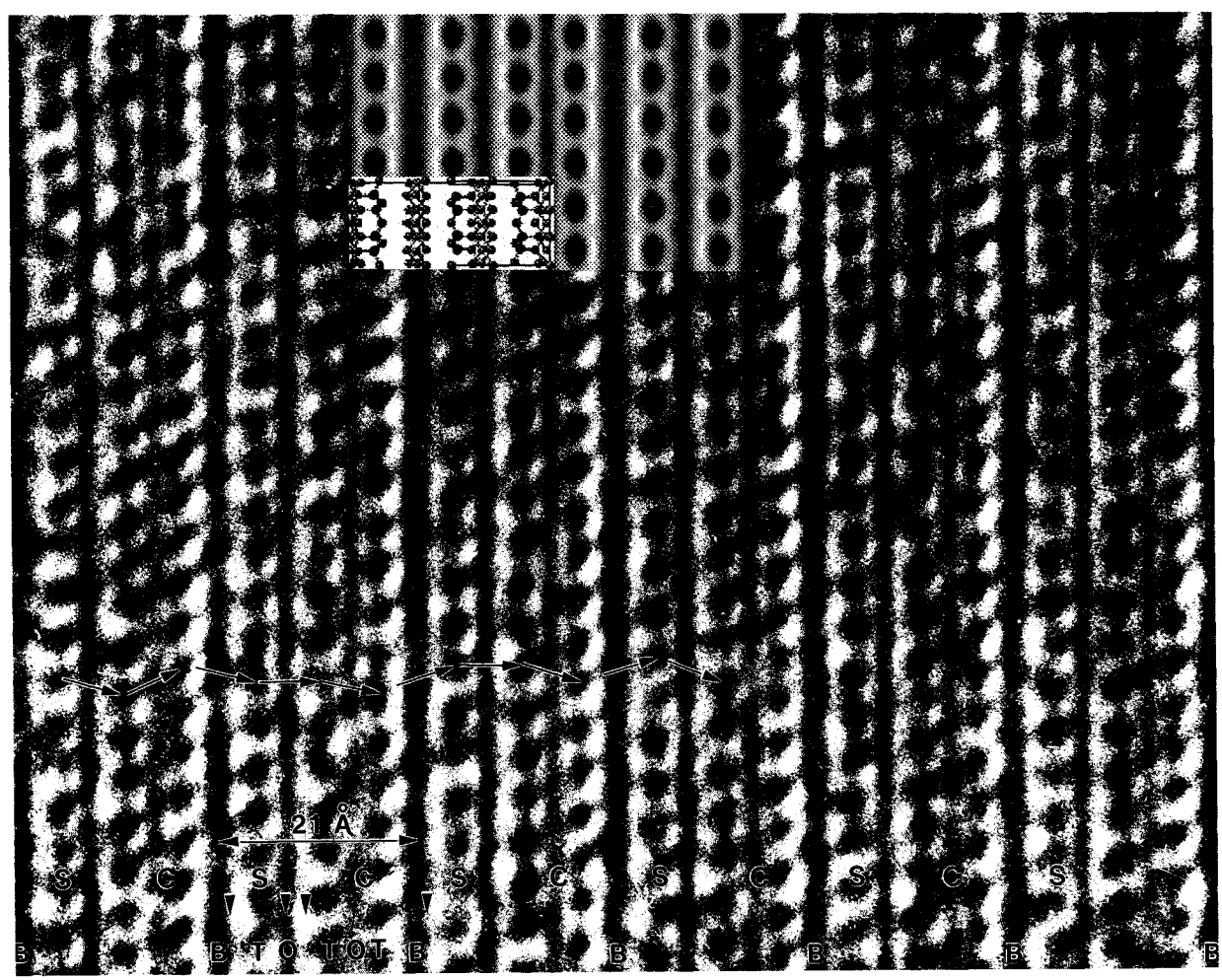

Fig. 4. HRTEM image down [100] of dozyite with superimposed image simulation and structural model. Correspondence between features in the experimental and calculated images verifies that dozyite is a regular interstratification of serpentine (S) and chlorite (C). Wide bands of very dark contrast correspond to the brucite-like interlayers, narrow medium-dark bands to the octahedral sheets within the 2:1 and 1:1 layers, and black spots to unresolved pairs of (Si,Al) tetrahedra. Arrows show that, in detail, tetrahedra are displaced from their ideal positions, indicating pervasive $\pm b/3$ disorder (see next figure).

peating chlorite layer must follow with zero shift of its lower sixfold ring relative to that of the serpentine layer in order to give the correct β angle. The $-a/3$ stagger of the 21-Å structure is provided entirely by the stagger within the 2:1 layer of the chlorite unit. No refinement of the structure has been attempted because of the streaking of $k \neq 3n$ reflections and the multiple nature of some of the $k = 3n$ reflections. The unrefined atomic coordinates are listed in Table 6.

The atomic coordinates of the monoclinic polytype I*aa*-2 were used in the model for intensity calculations for convenience because of the observed monoclinic shape of the unit cell. Note that, because of the random $\pm b/3$ shifts present in the dozyite crystals examined, the chlorite component within dozyite must be described as disordered in stacking also (i.e., in addition to shifts of $-a/3$ along all three pseudohexagonal **a** axes at random within the 2:1 layer, the interlayer must adopt all three *a* positions above the 2:1 layer at random), and the serpentine component then adopts all three *a* positions above the interlayer (equivalent to positions 2,4,6) at random. The entire assemblage should be described as a disordered I*aa*-(2,4,6) structure. The $k = 3n$ reflections are not affected by $b/3$ displacements, however, and so the $k = 3n$ intensities for the disordered structure are identical to those of the regular-stacking polytypes.

High-resolution transmission electron microscopy

High-resolution transmission electron microscopy (HRTEM) was employed to verify the structure of dozyite and to examine its abundance, distribution, and defect microstructures. Thin slices of sample approximately 1 mm in diameter allowed characterization of dozyite and coexisting interstratified materials. Details of the coexisting assemblages have been published separately (Banfield et al., 1994). Atomic-resolution images were interpreted by comparison with image simulations calculated using the proprietary program EMS (Stadelmann, 1991). Simulations were calculated using appropriate values for microscopic parameters (e.g., $C_s = 0.5$ mm, spread of focus = 10 nm, 1-mrad beam convergence) and sample thicknesses between 3 and 10 nm, at a range of defocal values (usually, -23, -33, -43, and -53 nm). Microscopy was performed using a Philips CM20UT with a point to point resolution of 0.19 nm.

HRTEM images demonstrated clearly that dozyite exists as discrete crystals rather than as regularly interstratified areas within serpentine, chlorite, or randomly interstratified material. Figure 4 is a high-resolution image of dozyite obtained down [100]. The superimposed image simulation calculated for the I*aa*-2 structure corresponds closely with the experimental image. The included structural representation illustrates that wide bands of very dark contrast correspond to brucite-like interlayers of the chlorite, narrow medium dark bands to octahedral sheets within the 2:1 and 1:1 layers, and black spots to unresolved pairs of Si,Al tetrahedra. Thus, the brucite-like interlayers and the 2:1 and 1:1 layers are clearly resolved.

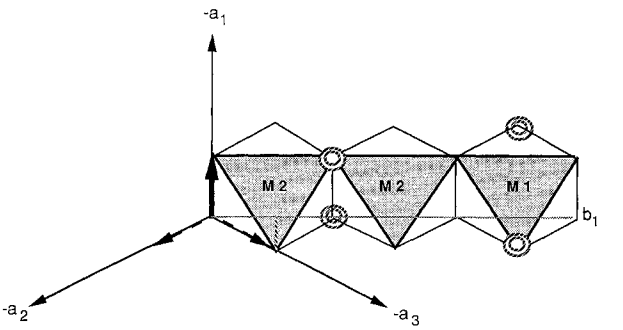

Fig. 5. Diagram illustrating that, when viewed down [100], $a/3$ disorder in tetrahedral positions appears as $b/6$ displacements. The double circles represent OH groups in cis orientation. The bold arrow represents a $-a_1/3$ shift within a 2:1 layer. If the interlayer shift instead had been $-a_3/3$, a tetrahedral cation attached to the apical O atom now at the upper left corner of the left M2 octahedron would be displaced to the bottom corner of that octahedron. Viewed along [100], this is a projected displacement of $b_1/6$.

These results confirm the X-ray-based model of dozyite as a regular interstratification of serpentine and chlorite.

If the detail in the HRTEM image in Figure 4 is compared carefully with the superimposed simulation, it is apparent that black spots on the image do not define straight lines parallel to [001], as in the simulation. This illustrates the difference between a regular-stacking I*aa*-2 structure, as in the simulation, and the actual semirandom-stacking I*aa*-(2,4,6) structure. In [100] projection, the three random $-a/3$ shifts mentioned above are oriented with one direction of shift normal to the plane of Figure 4 and the other two plunging $\pm 120°$ to the normal. The latter two shifts give apparent displacements of the tetrahedra of $\pm b/6$ in projection (Fig. 5). It should be noted that random adoption of the three possible *a* positions mentioned above creates random displacements of $\pm b/3$ of the chlorite interlayer sheet relative to the 2:1 layer on one side and to the 1:1 layer on the other side. These displacements create exactly the same effects on the image as the random $a/3$ shifts. Thus, the positions of the displaced tetrahedral units (black spots on the image in Fig. 4) vary in irregular but predictable fashion. The area shown in Figure 6 is quite typical, showing very regular alternation of serpentine and chlorite over large distances; however, the regular stacking along just one of the **a** axes is limited to only short distances.

Many areas of dozyite contain layer sequence errors. Typical examples include serpentine–brucitic interlayer–serpentine (serpentine tetrahedral sheets facing the brucitic interlayer on both of its sides) and 2:1–brucitic interlayer–2:1 sequences. Despite these defects, the regular alternation of tetrahedral and octahedral sheets (and the 21-Å periodicity of brucitic interlayers) is preserved. Figure 7 illustrates a region containing both of these mistakes. Beam damage (center of the image), focused by strain, marks the junction between reversed 2:1-serpentine and serpentine-2:1 packets. Other common defects

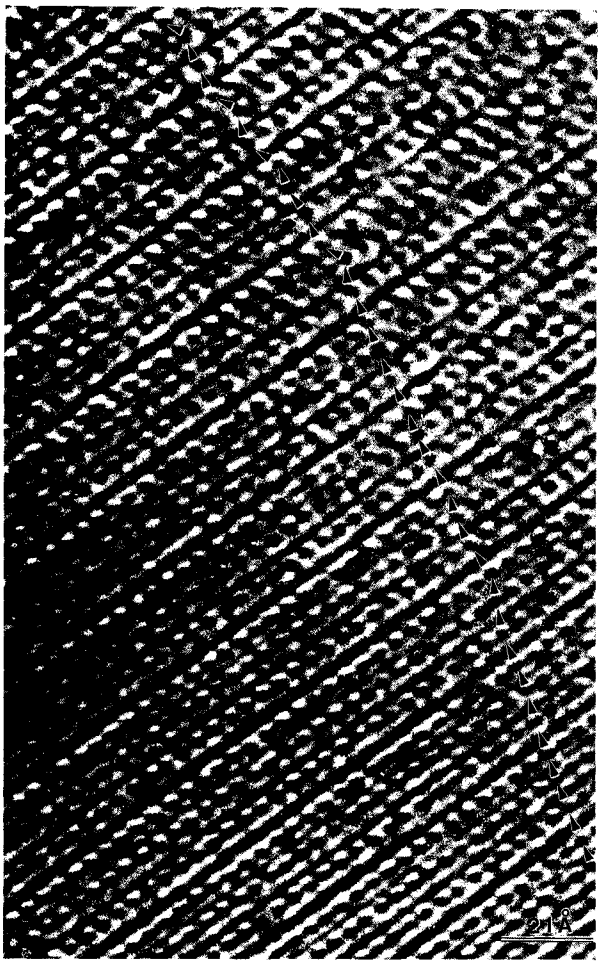

Fig. 6. HRTEM image down [100] of a typical well-ordered crystal. Note the abundant $b/3$ displacement disorder within 2:1 layers, between 2:1 and serpentine layers, and across the brucitic interlayer (illustrated by the random displacements of the dark spots).

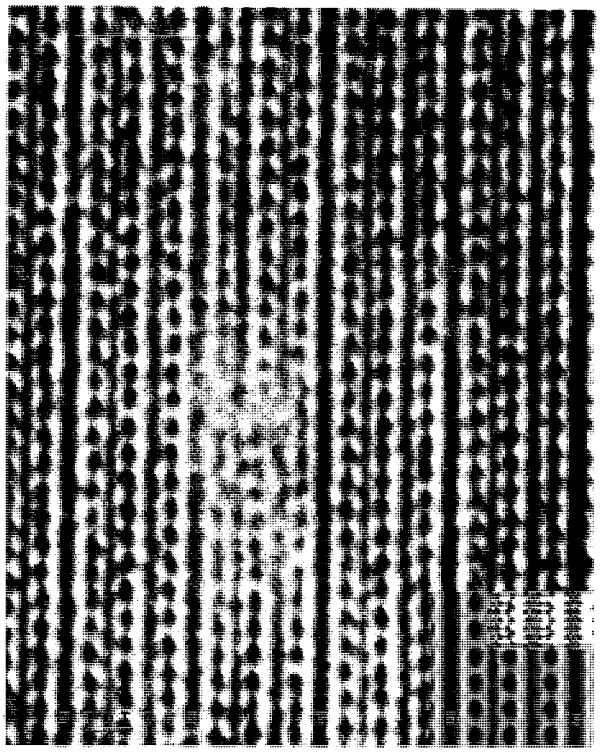

Fig. 7. HRTEM image down [100] with superimposed image simulation and structure representation showing layer repeat errors in dozyite. Beam-damaged area (low contrast near the center of the figure) marks the junction between reversed chlorite-serpentine and serpentine-chlorite sequences. Double arrows mark back to back serpentine 1:1 layers (OT) and single arrows mark back to back 2:1 layers (TOT) across brucitic interlayers (B).

within dozyite include incorporation of additional serpentine and chlorite units (Fig. 8).

Associated serpentine-chlorite phases

Several serpentine and chlorite polytypes as well as other regularly and randomly interstratified serpentine-chlorite phases are closely associated with dozyite. They are colorless to pale green and difficult to distinguish optically from dozyite and discrete chlorite or serpentine. Associated layer silicates were identified by X-ray Debye-Scherrer or precession photos of individual flakes or by electron diffraction and HRTEM study. The relative abundances of serpentine and chlorite (and of the interstratified minerals) vary dramatically over distances on the submillimeter scale. HRTEM samples with abundant dozyite typically contained both serpentine and chlorite. However, no correlations based on mineral abundances could be made.

The most abundant of the other regularly interstratified phases identified by both XRD and HRTEM techniques (<5% of the total) gives a diffraction pattern in which the $00l$ reflections and most other $k = 3n$ reflections have a 28-Å periodicity (vs. 21 Å for dozyite). HRTEM images show a regular sequence of two serpentine 1:1 layers and one chlorite unit. AEM analyses indicate a bulk composition more aluminian than for dozyite, in accord with the serpentine components being the Al-rich amesite. In addition, rare electron diffraction patterns were obtained from submicrometer-wide areas of phases with 35- and 42-Å periodicities. These and other associated minerals are described in a separate paper (Banfield et al., 1994).

It is of interest that although two structural types of chlorite can be identified in the assemblage coexisting with dozyite, II*bb* chlorite is the most abundant. We cannot establish with certainty that dozyite (for which the data indicate I*aa* chlorite to be present within its structure) formed by replacement of II*bb* chlorite because a second discrete one-layer chlorite (probably I*bb*) also was recognized. If I*aa* chlorite were not a precursor, formation of dozyite by replacement of II*bb* chlorite would require a shift of cations in the brucite-like interlayer (from *b* to *a* positions) and 180° rotation (probably through displacement of the coordinating anions) of the brucite-like interlayer (changing II to I).

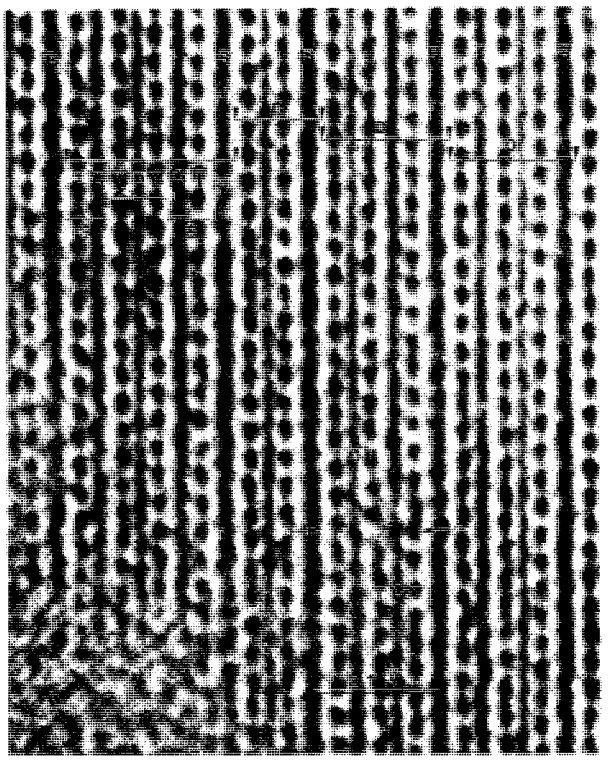

Fig. 8. HRTEM image down [100] showing layer repeat errors in the 21-Å phase (D), including extra chlorite (C) and serpentine layers (S). TOTOTOT marks a sequence 2.8 nm wide (see text). A defect that involves switching of the 2:1 and 1:1 sequences is marked by horizontal arrows. Low contrast at the bottom left of the figure is the ion-milled sample edge.

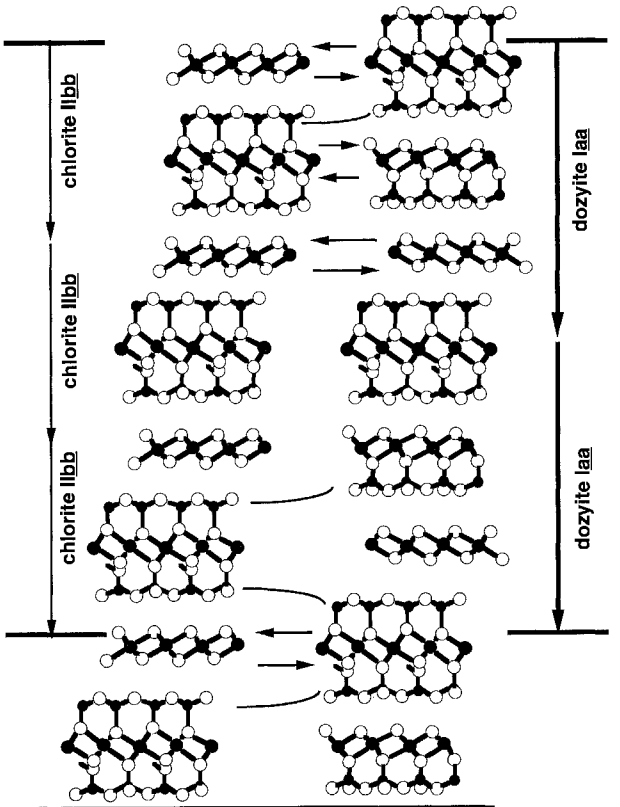

Fig. 9. Diagram down [010] showing the abundant chlorite polytype (II*b*) on the left and dozyite (I*aa*) on the right. Curved lines indicate where the tetrahedral sheets are inverted in the manner of Brindley and Gillery (1954). Arrows mark displacement of O planes necessary to convert type I to type II octahedral sheets. These displacements would not be necessary if the 21-Å phase replaces the other coexisting chlorite (I*b*). Unit-cell repeats are marked by vertical arrows.

Discussion

Dozyite has the distinction not only of representing a new mineral but of being the first layer silicate based on regular interstratification of two different layer types (1:1 and 2:1). Both XRD analysis and HRTEM imaging clearly indicate that the 21-Å periodicity of dozyite is due to the regular alternation of serpentine and chlorite units. Images show extensive disorder attributed to random *b*/3 displacements (involving tetrahedral positions) within the 2:1 layer, between the 2:1 layer and serpentine, and across the brucitic interlayer (Figs. 4 and 5). Other common defects include extra serpentine and chlorite units. HRTEM images verify that, although defects are present, dozyite crystals up to tens of micrometers wide are essentially composed of the regular serpentine-chlorite sequences (Fig. 6). Crystals of dozyite up to 2.0 mm in diameter exist on a macroscale, although most of these contain fine intergrowths of amesite as well.

Using AEM we have established that the composition of dozyite is well represented as a linear combination of the discrete amesite and clinochlore that are intimately associated with dozyite. Amesite is a relatively uncommon mineral (only four localities were reported by Bailey, 1988b, in the Mg-Al-Si system), normally restricted to very aluminous environments. The development of amesite in the Ertsberg East Complex skarn is surprising, given that geologic evidence suggests that the serpentine + chlorite assemblage replaced an Al-poor, magnesian calc-silicate assemblage. Our results, and those of Katchan (1982), support the hypothesis that the amesite and dozyite formed in an Al metasomatic event associated with the quartz monzonite intrusion.

The association of serpentine, clinochlore, dozyite, other regularly interstratified minerals, and randomly interstratified serpentine-chlorite clearly implies rampant disequilibrium. We suggest that, in addition to representing a polysomatic series, the clinochlore + dozyite + amesite assemblage may be described as a reaction series. Although we know little about the temperature and pressure of the reaction, we can infer from the textures that it involved the direct replacement of early chlorite by dozyite and then by amesite, rather than the chloritization of amesite.

The apparent limits of Al substitution in chlorites (Chernosky et al., 1988) and the implied compositional gaps between amesite and chlorite (Bailey, 1988b) and between amesite and aluminian lizardite (Bailey, 1988b)

may explain the development of regular amesite-clinochlore interstratifications. Although dozyite has a bulk composition within the attainable Si/Al range of chlorites, evidence from graphs such as that of Cathelineau and Nieva (1985) suggests that $^{[4]}$Al content is a function of temperature. We suggest, therefore, that conversion of clinochlore to amesite was driven primarily by Al activity under temperature and pressure conditions in which the maximum Al content of chlorite was quite limited. It is possible the dozyite grew by direct structural modification of existing chlorite. The inferred Al content of the chlorite component, which is close to that of coexisting clinochlore, implies little or no compositional modification of the original material. This reaction path may have promoted regular interstratification in place of development of discrete crystals of chlorite and amesite. Dozyite may be a kinetically favored reaction product because its formation can proceed by a modification of a subset of the structural units in chlorite (Fig. 9). The high activation barrier and lowered driving force may inhibit transformation of dozyite to sequentially more amesite-rich interstratifications, which are minor in amount, and ultimately to amesite.

We provide no direct evidence to rule out the formation of dozyite crystals by nucleation of separate crystals. In fact, the occurrence of discrete crystals rather than regularly interstratified zones may point to this mechanism of growth. Furthermore, it is clear that a possible Al-based compositional gap is not the only reason for formation of regular serpentine-chlorite interstratifications because we have established that dozyite occurs in at least two localities with very different parageneses. Dozyite from the Pennsylvania locality contains considerably less Al (even adding in the Cr), ruling out the possibility that it has an amesite component.

Acknowledgments

We are indebted to Robert C. Smith II for provision of the specimen of dozyite from the Wood Chrome mine. We thank John Fournelle for the electron probe analyses, Lee Riciputi for the ion probe analyses at Oak Ridge National Laboratory, and Gordon Medaris for the optical properties. This research was supported by a grant from the Department of Geology and Geophysics to S.W.B. and by NSF grant EAR-9117386 to J.F.B.

References cited

Ahn, J.H., and Peacor, D.R. (1985) Transmission electron microscopic study of diagenetic chlorite in Gulf Coast argillaceous sediments. Clay and Clay Minerals, 33, 228–236.

Amouric, M., Gianetto, I., and Proust, D. (1988) 7, 10 and 14Å mixed-layer phyllosilicates studied structurally by TEM in pelitic rocks of the Piemontese Zone (Venezuela). Bulletin de Minéralogie, 111, 29–37.

Bailey, S.W. (1982) Nomenclature for regular interstratifications. Clay Minerals 17, 243–248.

——(1988a) Chlorites: Structures and crystal chemistry. In Mineralogical Society of America Reviews in Mineralogy, 19, 347–403.

——(1988b) Structures and compositions of other trioctahedral 1:1 phyllosilicates. In Mineralogical Society of America Reviews in Mineralogy, 19, 169–188.

——(1988c) Odinite, a new dioctahedral-trioctahedral Fe^{3+}-rich 1:1 clay mineral. Clay Minerals, 23, 237–247.

——(1988d) X-ray diffraction identification of the polytypes of mica, serpentine, and chlorite. Clays and Clay Minerals, 36, 193–213.

Bailey, S.W., and Brown, B.E. (1962) Chlorite polytypism: I. Regular and semi-random one-layer structures. American Mineralogist, 47, 819–850.

Bailey, S.W., and Tyler, S.A. (1960) Clay minerals associated with the Lake Superior iron ores. Economic Geology, 55, 150–175.

Banfield, J.F., Bailey, S.W., and Barker, W.W. (1994) Polysomatism, polytypism, defect microstructures, and reaction mechanisms in regularly and randomly interstratified serpentine and chlorite. Contributions to Mineralogy and Petrology, 117, 137–150.

Brindley, G.W., and Gillery, F.H. (1954) A mixed-layer kaoline-chlorite structure. Clays and Clay Minerals, 2, 349–353.

Cathelineau, M., and Nieva, D. (1985) A chlorite solid solution geothermometer. Contributions to Mineralogy and Petrology, 91, 235–244.

Chernosky, J.V., Jr., Berman, R.G., and Bryndzia, L.T. (1988) Stability, phase relations, and thermodynamic properties of chlorite and serpentine group minerals. In Mineralogical Society of America Reviews in Mineralogy, 19, 295–346.

Dean, R.S. (1983) Authigenic trioctahedral clay minerals coating Clearwater Formation sand grains at Cold Lake, Alberta, Canada. Programs and Abstracts, 20th Annual Meeting of the Clay Minerals Society, Buffalo, New York, 79.

Foster, M.D. (1962) Interpretation of the composition and classification of the chlorites. U.S. Geological Survey Professional Paper 414-A, 1–33.

Gillery, F.H. (1959) The X-ray study of synthetic Mg-Al serpentines and chlorites. American Mineralogist, 44, 143–152.

Hall, S.H., Guggenheim, S., Moore, P., and Bailey, S.W. (1976) The structure of Unst-type 6-layer serpentines. Canadian Mineralogist, 14, 314–321.

Hillier, S., and Velde, B. (1992) Chlorite interstratified with a 7 Å mineral: An example from offshore Norway and possible implications for the interpretation of the composition of diagenetic chlorites. Clay Minerals, 27, 475–486.

Jahren, J.S., and Aagaard, P. (1989) Compositional variation in diagenetic chlorites and illites, and relationships with formation-water chemistry. Clay Minerals, 24, 157–170.

James, R.S., Turnock, A.C., and Fawcett, J.J. (1976) The stability and phase relations of iron chlorite below 8.5 kb P_{H_2O}. Contributions to Mineralogy and Petrology, 56, 1–25.

Jiang, S., Zhang, G., Qi, J., and Liu, W. (1982) Discovery of new types of regularly interstratified septechlorite-swelling chlorite and chlorite-antigorite in China. Acta Petrologica Mineralogica et Analytica, 1, 36–43 (in Chinese).

Jiang, W.-T., Peacor, D.R., and Slack, J.F. (1992) Microstructures, mixed layering, and polymorphism of chlorite and retrograde berthierine in the Kidd Creek massive sulfide deposit, Ontario. Clays and Clay Minerals, 40, 501–514.

Katchan, G. (1982) Mineralogy and geochemistry of the Ertsberg (Gunung Bijih) and Ertsberg East (Gunung Bijih Timur) skarns, Irian Jaya, Indonesia, and the OK Tedi skarns, Papua New Guinea, 498 p. Ph.D. thesis, University of Sydney, Sydney, New South Wales, Australia.

Lee, J.H., and Peacor, D.R. (1983) Interlayer transitions in phyllosilicates of Martinsburg shale. Nature, 303, 608–609.

MacKinney, J.A., Mora, C.I., and Bailey, S.W. (1988) Structure and crystal chemistry of clintonite. American Mineralogist, 73, 365–375.

Moore, D.M., and Hughes, R.E. (1991) Characteristics of chlorite interlayered with a 7 Å mineral as found in sandstone reservoirs. Programs and Abstracts, 28th Annual Meeting of the Clay Minerals Society, Houston, Texas, 115.

Nelson, B.W., and Roy, R. (1958) Synthesis of the chlorites and their structural and chemical constitution. American Mineralogist, 43, 707–725.

Odin, G.S., Bailey, S.W., Amouric, M., Fröhlich, F., and Waychunas, G.S. (1988) Mineralogy of the verdine facies. In G.S. Odin, Ed., Developments in sedimentology, 45, p. 159–206. Elsevier, Amsterdam.

Reynolds, R.C., Jr. (1988) Mixed layer chlorite minerals. In Mineralogical Society of America Reviews in Mineralogy, 19, 601–629.

Reynolds, R.C., Jr., DiStefano, M.P., and Lahann, R.W. (1992) Random-

ly interstratified serpentine/chlorite: Its detection and quantification by powder X-ray diffraction methods. Clays and Clay Minerals, 40, 262–267.

Shirozu, H., and Momoi, H. (1972) Synthetic Mg-chlorites in relation to natural chlorite. Mineralogical Magazine (Japan), 6, 464–476.

Slack, J.F., Jiang, W.-T., Peacor, D.R., and Okita, P.M. (1992) Hydrothermal and metamorphic berthierine from the Kidd Creek volcanogenic massive sulphide deposit, Timmons, Ontario. Canadian Mineralogist, 30, 1127–1142.

Stadelmann, P. (1991) Simulation of HREM images and 2D CBED patterns using EMS software package. Software manual 12M-EPFL, Lausanne, Switzerland.

Walker, J.R, and Thompson, G.R. (1990) Structural variations in chlorite and illite in a diagenetic sequence from the Imperial Valley, California. Clays and Clay Minerals, 38, 315–321.

Wicks, F.J., and O'Hanley, D.S. (1988) Serpentine minerals: Structures and petrology. In Mineralogical Society of America Reviews in Mineralogy, 19, 91–167.

Yau, Y.-C., Peacor, D.R., Beane, R.E., Essene, E.J., and McDowell, S.D. (1988) Microstructure, formation mechanisms, and depth-zoning of phyllosilicates in geothermally altered shales, Salton Sea, California. Clays and Clay Minerals, 36, 1–10.

Yoder, H.S., Jr. (1952) The MgO-Al_2O_3-SiO_2-H_2O system and related metamorphic facies. American Journal of Science, Bowen Volume, 569–627.

Zheng, H., and Bailey, S.W. (1989) Structures of intergrown triclinic and monoclinic II*b* chlorites from Kenya. Clays and Clay Minerals, 37, 308–316.

Manuscript received August 23, 1993
Manuscript accepted September 20, 1994